

Analysis of Jupiter's deep jets combining Juno gravity and time varying magnetic field measurements

Keren Duer¹, Eli Galanti¹ and Yohai Kaspi¹

(Astrophysical Journal Letters, in press)

June 20, 2019

¹*Department of Earth and Planetary Sciences, Weizmann Institute of Science, Rehovot, Israel.*

Abstract

Jupiter's internal flow structure is still not fully known, but can be now better constrained due to Juno's high-precision measurements. The recently published gravity and magnetic field measurements have led to new information regarding the planet and its internal flows, and future magnetic measurements will allow taking another step in resolving this puzzle. In this study, we propose a new method to better constrain Jupiter's internal flow field using the Juno gravity measurements combined with the expected measurements of magnetic secular variation. Based on a combination of hydrodynamical and magnetic field considerations we show that an optimized vertical profile of the zonal flows that fits both measurements can be obtained. Incorporating the magnetic field effects on the flow better constraints the flow decay profile. This will allow getting closer to answering the long-lived question regarding the depth and nature of the flows on Jupiter.

1 Introduction

The nature of Jupiter's interior is still a great mystery. The recent discovery that the depth of Jupiter's surface winds is ~ 3000 km (Kaspi et al., 2018) raises the possibility that the flow penetrates to depths where the electrical conductivity is large enough so that the flow might interact with the magnetic field. Due to Jupiter's large mass and density, the inner pressure is high enough to cause gas ionization relatively close to its surface. The significant ionization is expected at ~ 0.97 of the radius of Jupiter (~ 2000 km from its surface), getting stronger with depth (Liu et al., 2008; French et al., 2012). According to the Juno gravity field measurements (Kaspi et al., 2018) the flow is expected to penetrate the ionized region and therefore influence the magnetic field and vice versa.

The electromagnetic (EM) induction equation describes the temporal variability of the magnetic field due to interaction with the flow, the strength of the magnetic field itself and the electrical conductivity of the fluid. Since the electrical conductivity at Jupiter's higher atmosphere (cloud-level to ~ 2000 km) is very low (Liu et al., 2008; French et al., 2012), the jet streams are expected to have no interaction with the magnetic field. In this region, the flows have a significant effect on the gravity field (Kaspi, 2013; Kaspi et al., 2018). The inner region, below ~ 2000 km with remnants of jet velocities, is associated with an electrical conductivity that increases exponentially with depth, and might affect magnetic field anomalies (Galanti et al., 2017b). Note that the transition between the two regions is likely gradual and not abrupt.

Several studies examined the possible interaction between the flow and the magnetic field in gas giants (e.g., Liu et al., 2008; Gastine and Wicht, 2012; Jones, 2014; Cao and Stevenson, 2017; Dietrich and Jones, 2018), but none have used the gravity and magnetic field measurements simultaneously to add constraints to the possible flow profile in Jupiter and other gaseous planets. Previous studies that estimated the flow decay structure have not considered the interaction between the flow and magnetic fields (e.g., Kaspi et al., 2018). One study presented the mean-field electrodynamic balance (MFED) as a method for constraining the deeper regions of the decay flow profile (Galanti et al., 2017b), but it is likely that due to the Juno measurements showing strong azimuthal variations in the magnetic field, the magnetic field of Jupiter is too complicated for using the MFED method. Use of this method will result in different vertical structure for each longitude, which is highly unconstrained. Conversely, the time changes

in the magnetic field (also named magnetic secular variation), are likely to be measurable within the upcoming Juno measurements (Moore et al., 2018), and might be used to better constrain the flow field.

Temporal variation in the magnetic field generated by the core dynamo has been also identified for the Earth (e.g., Vestine and Kahle, 1966; Kahle et al., 1967; Bloxham and Gubbins, 1985), and estimated for other planetary interiors such as Jupiter’s (e.g., Gastine et al., 2014; Jones, 2014; Ridley and Holme, 2016). On Earth, the secular variation (SV) is exploited to yield flow profiles at the top of Earth’s outer core (Bloxham and Gubbins, 1985; Bloxham, 1992). While on Earth the SV strongly indicates internal flows in the core (Holme and Olson, 2007), in Jupiter the SV can be a result of multiple origins, among them interior flows in the fully conductive region, external sources and zonal flows in the semi conductive region (Gastine et al., 2014; Ridley and Holme, 2016). SV time scale associated with zonal flows for Jupiter’s magnetic field is estimated to be notable even within a single year (Gastine et al., 2014; Moore et al., 2018, 2019), if measured with high enough resolution. Moore et al. (2019) show that time variations in Jupiter’s internal magnetic field recorded from different spacecrafts (from Pioneer 10 until Juno) over the past 50 years are consistent with advection by zonal flows. However, since Juno revealed a complex longitudinal structured magnetic field, it is possible that using all passes of the Juno mission itself will allow tracking the advection of these longitudinal features and better estimation of the vertical profile of the zonal flows.

In this study, we use the recently published gravity measurements from Juno (Iess et al., 2018), together with the magnetic field measurements (Connerney et al., 2018) and the upcoming time-varying magnetic field measurements to better understand the nature of the deep flows in Jupiter. We present a method for the calculation of the decay profile of Jupiter’s surface winds that can explain both the Juno gravity measurements and the time-varying magnetic measurements, which are currently measured by Juno. The latter are simulated and used to constrain the lower region of the flow decay profile by the EM induction equation that relates the magnetic secular variation to the flow strength. The upper region associated with strong flows is determined by relating the gravity field to the flows via thermal wind balance (Kaspi et al., 2010). We also characterize the transition between the regions using a variety of flow decay options and multiple transition options to find the best solution that can fit both measurements.

The manuscript is organized as follows: in section 2 we present the relation connecting the flow field and the gravity (aka thermal wind (TW) balance), and the magnetic secular variation (MSV) model, and describe the simulation and optimization processes. In section 3 the combined solution based on both gravity and magnetic fields is presented, and in section 4 we discuss the implications of this study and conclude.

2 Methodology

In order to better constrain the deep flow on Jupiter, we combine two fundamentally different approaches. The first is based purely on the gravity measurements and their relation to the flow via TW balance (e.g., Kaspi, 2013; Galanti et al., 2017b; Kaspi et al., 2018), and the other is based on the EM induction equation called the MSV method (Bloxham and Gubbins, 1985; Bloxham, 1992). We aim to use the gravity constraints to find the best solution for the upper region of the flow, and the MSV method to better constrain the lower region of the flow and the transition between the regions.

2.1 Gravity field constraints

Jupiter’s large size and rapid rotation imply that the leading order momentum balance is geostrophic, namely a balance between the Coriolis force and the horizontal pressure gradients (Vallis, 2006). Consequently, the leading order vorticity balance is thermal wind balance (Kaspi et al., 2009). The zonal (azimuthal) component of the thermal wind balance is

$$2\Omega \frac{\partial}{\partial z} (\tilde{\rho}u) = \tilde{g} \frac{\partial \rho'}{\partial \theta}, \quad (1)$$

where Ω is the planetary rotation rate of Jupiter ($\frac{2\pi}{\Omega} \cong 9.92$ h), z is the direction parallel to the spin axis, $u(r, \theta)$ is the zonal flow, with θ being latitude and r is the depth, $\tilde{\rho}(r)$ is the background radially dependent density field, $\tilde{g}(r)$ is the corresponding radial gravitational acceleration and $\rho'(r, \theta)$ is the density anomaly related to the zonal flow. Expanding to higher order balances, beyond thermal wind, including the contributions due to oblateness, is possible, but it has been shown that for determination of the deep flows, thermal wind balance (Eq. 1) is the leading order balance and is sufficient (Galanti et al., 2017a).

The zonal gravitational harmonics, induced by the dynamics, are calculated by integrating the density anomaly ρ' from Eq. 1 (Kaspi et al., 2010). They are represented by

$$\Delta J_n^{\text{mod}} = -\frac{2\pi}{MR_J^n} \int_0^{R_J} r^{n+2} dr \int_{s=-1}^1 P_n(s) \rho'(r, s) ds, \quad (2)$$

where ΔJ_n^{mod} , $n = 2, \dots, N$ are the harmonic gravity coefficients induced by the zonal flows, M and R_J are Jupiter's mass and radius, respectively, P_n are the associated Legendre polynomials and $s = r \cos(\theta)$. The gravity harmonics can be used to calculate the latitude-dependent gravity anomalies in the radial direction $\Delta g_r^{\text{mod}}(\theta)$, so representation of the model results is available in both terms (Kaspi et al., 2010; Galanti et al., 2017c).

Giant planets are, to leading order, north-south symmetric bodies. The value of the low-degree even gravity harmonics reflect mostly the internal mass distribution within the planet, resulting from the planet's shape and rotation (Hubbard, 2012). Therefore, the even degrees ($n = 2, 4, 6, \dots$) resulting from the flow are difficult to be differentiated from the total values and might not be a good indicator for the dynamics (Kaspi, 2013; Kaspi et al., 2017). If no north-south asymmetry exists, the odd J_n should be identically zero. Juno was able to measure all the gravity harmonics within the sensibility range (Iess et al., 2018; Kaspi et al., 2018), and found significant non-zero values for the odd gravity harmonics. Since rigid body rotation cannot explain these values, wind asymmetry between the hemispheres must be the cause for the odd J_n . Consequently, for the odd harmonics $\Delta J_n = J_n$. Following Kaspi et al. (2018), we use the TW approach to calculate the flow decay profile that can explain the four odd gravitational moments (J_3, J_5, J_7 , and J_9) within the uncertainty range. Unlike Kaspi et al. (2018), we also require that this profile is physically consistent with magnetic field considerations as described below.

2.2 Time dependent magnetic field constraints

The temporal variation of Jupiter's magnetic field can be described by the Maxwell equations, combined to set the EM induction equation (e.g., Jones, 2011),

$$\frac{\partial \mathbf{B}}{\partial t} = \nabla \times (\mathbf{u} \times \mathbf{B}) - \nabla \times (\eta \nabla \times \mathbf{B}), \quad (3)$$

where \mathbf{B} is the three dimensional magnetic field, \mathbf{u} is the three dimensional velocity and $\eta = \frac{1}{\mu_0 \sigma}$ is the magnetic diffusivity, with μ_0 being the magnetic permeability of free space and $\sigma(r)$ is the electrical conductivity.

If Jupiter's internal flow indeed extends down to regions of high electrical conductivity, a non-negligible effect on the time dependent magnetic field is expected. This effect is not the only one that can cause magnetic secular variation, and other effects such as an external magnetodisk (Ridley and Holme, 2016), internal dynamo variabilities (Jones, 2014; Dietrich and Jones, 2018) or other rotation periods (Moore et al., 2019) are possible. However, within the time scales we are addressing, zonal flow advection is the predominant one. Considering only steady zonal flows are considered, the non-linear interaction term between the flow field and the magnetic field in the radial direction becomes

$$-\frac{u}{r \sin \theta} \frac{\partial B_r}{\partial \phi}, \quad (4)$$

where ϕ is longitude, θ here is co-latitude and $\frac{u}{r \sin(\theta)}$ is the angular velocity associated with the zonal flows. The magnetic field can be decomposed into poloidal and toroidal components such that

$$\mathbf{B} = \nabla \times (\nabla \times P \mathbf{e}_r) + \nabla \times T \mathbf{e}_r, \quad (5)$$

where P and T are the poloidal and toroidal potentials, respectively..

Similar to the gravity decomposition, the EM induction equation is solved with a pseudo-spectral method. Using spherical harmonics in the horizontal directions and Chebyshev polynomials in the radial direction, the poloidal potential is then

$$P = \sum_n \sum_l \sum_m P_{lmn} C_n(r) Y_l^m(\theta, \phi), \quad (6)$$

where $C_n(r)$ are the Chebyshev polynomials of degree n , $Y_l^m(\theta, \phi)$ are the spherical harmonics of degree l and order m , and P_{lmn} are the coefficients associated with each combination of the Chebyshev and spherical harmonic functions. For the toroidal potential an equivalent equation is used. Note that representation of the potentials is

possible also with the Schmidt coefficients as in Connerney et al. (2018). The poloidal magnetic potential governing equation then becomes

$$\frac{l(l+1)}{r^2} \left[\left(\frac{\partial}{\partial t} + \lambda \frac{l(l+1)}{r^2} \right) C_n - \lambda C_n'' \right] P_{lmn} = - \int Y_l^{m*} \frac{u}{r \sin \theta} \frac{\partial B_r}{\partial \phi} d\Omega. \quad (7)$$

where the double prime denotes second derivative in r , $\lambda = \frac{\eta}{\eta_{\text{bottom}}}$ is the normalized magnetic diffusivity and Ω is the solid angle. Juno was able to measure the three components of the magnetic field outside of Jupiter (the scalar potential field) in the first year of orbit (Connerney et al., 2018), which can be used to construct a map of the averaged B_r during the first year of measurements (the Juno reference model through Perijove 9 - JRM9). In the following orbits, Juno will continue to measure the scalar potential of Jupiter’s magnetic field to yield a new map of the averaged B_r during this time. If there will be a notable change in the spatial structure of B_r between the two periods, the induction relation can be used to determine the vertical profile of the flow. We search for a flow decay profile that will generate changes in the magnetic field (and therefore in P and T) that will best fit the measured time changes in B_r .

2.3 Simulation and measurements

Since the gravity measurements are already available (Iess et al., 2018), while the temporal variation in the magnetic field is not, validation of the solution is possible only with respect to one of the two measurements that we aim to explain. In order to test the methodology presented here, we simulate the time varying magnetic field measurements. The simulated measurements are generated by integrating the induction equation (Eq. 3) with a chosen flow structure (\mathbf{u} in Eq. 3) for approximately one year.

Using the decay profile of Kaspi et al. (2018) is found to be inconsistent with the time changing magnetic field. The resulting time variation in the magnetic field, after integrating the induction model for one year, is too large and not physical (not shown). This by itself indicates that the Kaspi et al. (2018) profile is too strong in regions of high electrical conductivity and hence cannot be used to constrain the flow at depths below ~ 3000 km. Moreover, any solution that includes substantial deeper zonal flows will be inconsistent with the magnetic field constraints (e.g., Kong et al., 2018).

Therefore, we define a modified decay profile that is similar to the Kaspi et al. (2018) profile above ~ 2000 km and weaker below (Fig. 1), yet still generates reasonable gravity harmonics (Table 1). The induction model is then integrated with the new profile to create “measurements” of the time varying magnetic field according to Eq. 3-7. We set this decay profile with a relatively small number of parameters, but with enough freedom to contain the needed complexity. The upper region is similar to Kaspi et al. (2018), and the lower region is a simple exponential decay, so that the overall simulated flow structure is

$$U_s(\theta, r) = U_{\text{surf}}(s) Q_s(r), \quad (8)$$

$$Q_s(r) = (1 - \alpha) \exp\left(\frac{r - R_J}{H_1}\right) + \alpha \left[\frac{\tanh\left(\frac{-R_J - H_2 - r}{\Delta H}\right) + 1}{\tanh\left(\frac{H_2}{\Delta H}\right) + 1} \right] \quad R_T \leq r \leq R_J, \quad (9)$$

$$Q_s(r) = Q_s(r = R_T) \exp\left(\frac{r - R_T}{H_3}\right) \quad r < R_T, \quad (10)$$

where $U_{\text{surf}}(s)$ is the measured wind at R_J (Tollefson et al., 2017) projected toward the planet’s interior in the direction parallel to the spin axis, $Q_s(r)$ is the radial decay simulated function (Fig. 1), and the set of parameters that forms the decay rate are: $\alpha = 0.5$, $H_1 = 2389$, $H_2 = 1830$ km, $\Delta H = 500$ km, $R_T = 0.958R_J$ and $H_3 = 660$ km.

Interestingly, it appears that J_3 is very sensitive to depths of 2500–4000 km and that a weak flow at those depths does not allow fitting J_3 to the Juno measurements. Combined with the fact that the induction model requires very weak flow below 3500 km, in order to generate reasonable changes in the magnetic field, we find that J_3 constrains the flow to reach deeper than 3500 km, but the flow at those depths cannot be higher than $\sim 5 - 10 \text{ ms}^{-1}$, and can reach no more than $\sim 1 \text{ ms}^{-1}$ at 5000 km.

Due to Jupiter’s large mass, its electrical conductivity is relatively high close to its surface. To date, Jupiter’s electrical conductivity profile in the upper 5000 km of the planet is based mostly on ab initio simulations and shock wave experiments (Nellis et al., 1992, 1995; Weir et al., 1996; Liu et al., 2008; French et al., 2012). The latest published magnetic field (Connerney et al., 2018) combined with the induction model in this study, requires relatively low conductivity at depths of 2000 – 5000 km, to allow reasonable changes in the magnetic field with

time. The conductivity profile chosen here is similar to the profile of Cao and Stevenson (2017), and is within the error range of the Liu et al. (2008) profile (Fig. 1). We model the magnetic diffusivity (the inverse of the electrical conductivity) similar to Jones (2014); Cao and Stevenson (2017) and Dietrich and Jones (2018) such that:

$$\eta(r) = F \cdot \exp\left(c + \sqrt{c^2 + d}\right) \quad (11)$$

where $c = \frac{1}{2}[(g_1 + g_3)r - g_2 - g_4]$, $d = (g_1r - g_2)(g_3r - g_4) - g_5$, $F = 10$, $g_1 = 645.81$, $g_2 = 611.42$, $g_3 = 246.03$, $g_4 = 222.54$ and $g_5 = 0.21919$.

Table 1 | The Juno-measured and models odd gravity harmonics

Harmonic	Measured	Kaspi et al. 2018	Simulation	Model solution
$J_3(\times 10^{-8})$	-4.24 ± 0.91	-5.71 ± 1.67	-1.72	-4.48
$J_5(\times 10^{-8})$	-6.89 ± 0.81	-7.73 ± 0.41	-7.61	-7.69
$J_7(\times 10^{-8})$	12.39 ± 1.68	12.77 ± 0.54	10.87	12.42
$J_9(\times 10^{-8})$	-10.58 ± 4.35	-8.84 ± 0.42	-7.11	-9.02

Table 1: The measured odd gravity harmonics from Juno, the Kaspi et al. (2018) model results, the simulated profile and the new combined model results. The uncertainties are the 3σ uncertainty values for the measurements and the Kaspi et al. (2018) model.

The changes in the radial component of the magnetic field resulting from the simulated decay profile are shown in Fig. 2b, along with the measured B_r from Juno’s first nine orbits (Fig. 2a) (Connerney et al., 2018), and the simulated flow that caused this change (Fig. 2c). Both magnetic fields (Fig. 2a,b) are constructed with only 10 degrees of freedom of the harmonic coefficients l and m , as in Connerney et al. (2018). The strongest changes in the magnetic field appear at latitudes $0 - 20^\circ\text{N}$ and are caused due to flows that penetrate areas of high electrical conductivity (Fig. 2c). The cylindrical projection of the surface winds, parallel to the axis of rotation, causes the strong jet at 20°N at the surface to shift equatorward and causes the strong variation in B_r at $\sim 10^\circ\text{N}$. We will next consider this time varying magnetic field as an example for the expected Juno measurements.

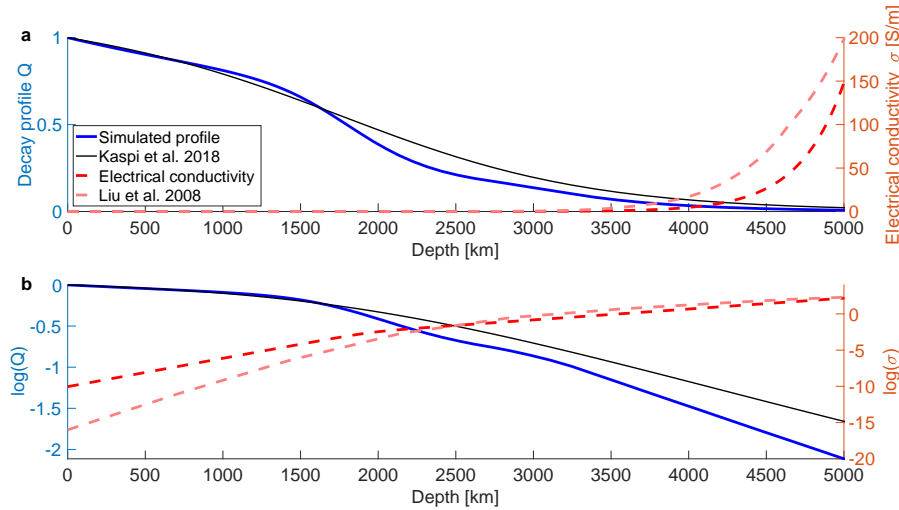


Figure 1: The decay profile of Kaspi et al. (2018) (black), the simulated decay profile used to generate the $\frac{\partial B}{\partial t}$ measurements (blue), the electrical conductivity (dashed red) and the electrical conductivity as appears in Liu et al. 2008 (light dashed red) in linear (a) and log scales (b).

2.4 The combined gravity-magnetic optimization

The measurements of the magnetic field, given at the planet’s surface, can be projected in the radial direction to the regions where the conductivity is no longer negligible (Galanti et al., 2017b), according to potential field

continuation. The comparison between the model and the measurement should be at this depth, chosen here as $R_c = 0.972R_J$ as in Galanti et al. (2017b). We choose to fit the measurements with a simple exponential decay flow profile in the regions of the induction model as we expect that the strong electrical conductivity in this region will cause the flow to dissipate fast and proportionally to the electrical conductivity itself which is also exponential. The flow in this region is modeled such that

$$U_{\text{Model}}(\theta, r) = U_{\text{surf}}(s)Q_M(r), \quad (12)$$

$$Q_M(r) = U_M \exp\left(\frac{r - 0.972R_J}{H_M}\right) \quad 0.93R_J \leq r \leq 0.972R_J, \quad (13)$$

where U_M is the flow strength at $r = 0.972R_J$ relative to the surface flow and H_M is the exponential decay rate. The search for the best solution is made by comparing the resulting changes in the magnetic field from the model to the simulation. Each model run with different U_M and H_M , using a cost-function (scalar measure) to find the best solution. The cost-function is defined as

$$L_{\text{MSV}} = \sum_{n=1}^{10} \sum_{m=0}^n \left[\left(\frac{\partial g_{nm}^{\text{sim}}}{\partial t} - \frac{\partial g_{nm}^{\text{mod}}}{\partial t} \right)^2 + \left(\frac{\partial h_{nm}^{\text{sim}}}{\partial t} - \frac{\partial h_{nm}^{\text{mod}}}{\partial t} \right)^2 \right] \quad 0.93R_J \leq r \leq 0.972R_J, \quad (14)$$

where g_{nm}^{sim} and h_{nm}^{sim} are the simulated harmonic Schmidt coefficients (Connerney et al., 2018) at the upper boundary of the model and g_{nm}^{mod} and h_{nm}^{mod} are the model solution for those coefficients (not to be confused with the gravity anomaly Δg_r). We then define the model solution as the average between all the solutions of the lowest order of magnitude of the resulting cost-function.

We define the transition between the MSV model and the TW model as a distinct boundary (R_T), which needs to be set in the optimization process. For the upper region of the solution ($R_T < r \leq R_J$), we use the TW inversion approach (Galanti and Kaspi, 2016, 2017), fitting the gravity odd harmonics that resulted from the forward model to the measured ones, using a second cost-function,

$$L_{\text{TW}} = \sum_{i=3,5,7,9} \sum_{j=3,5,7,9} w_{ij} (J_i^{\text{obs}} - J_i^{\text{mod}}) (J_j^{\text{obs}} - J_j^{\text{mod}}) \quad R_T \leq r \leq R_J, \quad (15)$$

where J_n^{obs} are the Juno measurements, J_n^{mod} are the model solutions and w_{ij} is the 4×4 weight matrix as in Kaspi et al. (2018). In the upper region, we find the best fit by optimizing the decay profile independently at each vertical grid point of the model, demanding that the vertical structure function Q is 1 at R_J and has the value of the resulted flow strength from the MSV model at the transition depth $Q_M(R_T)$. We also demand that the vertical structure function decreases monotonically with depth. The decay profile in the region between the transition depth and the upper boundary of the Induction model ($R_T \leq r \leq 0.972R_J$) is recalculated with the TW model. However, this region is still aligned with considerable conductivity, therefore we must recalculate the changes in the magnetic field to make sure that the solution is still compatible with the measurements. The value of the transition depth between the models (R_T) is determined as deep as possible with the requirement that the time varying magnetic field results remain valid.

3 Results

We start with the optimization of the lower region of the decay profile using the MSV model. The cost function (Eq. 14) shows a near linear relation between the parameters U_M and H_M (Fig. 3b). Since an optimal solution in the global minimum is not a unique point but an area (blue region in Fig. 3b), we average the lowest order of magnitude of solutions (pink and red dots in Fig. 3b) to determine the optimal decay rate in the inner layers (Fig. 3a, green line). The solution is obtained with $U_M = 0.6514$ and $H_M = 0.66$. The resulting model solution (green line) is very far from the simulated decay profile (black dashed line) in the region of 2000 – 3000 km, but converges to the simulated decay profile deeper than ~ 3000 km. This suggests that the transition depth (R_T , Eq. 15) should be deeper than ~ 3000 km ($\cong 0.958R_J$), chosen here as $R_T = 3500$ km ($\cong 0.95R_J$).

Next, using the TW model, we find a solution for the decay profile that is constrained with the MSV solution at $R_T = 0.95R_J$. The new solution fits both the Juno measurements and the simulation for the changes in the magnetic field (Fig. 3a, red). This combined gravity-magnetic solution shows a unique pattern of two rapid and perhaps unrelated decay patterns. The first, close to the cloud-level, might account for a baroclinic atmospheric outer layer (e.g., Kaspi and Flirel, 2007) that decays until reaching a nearly barotropic state; and the second, around $H = 3500$ km, that could reflect the magnetic braking. However, the first decay is very close to the cloud-level

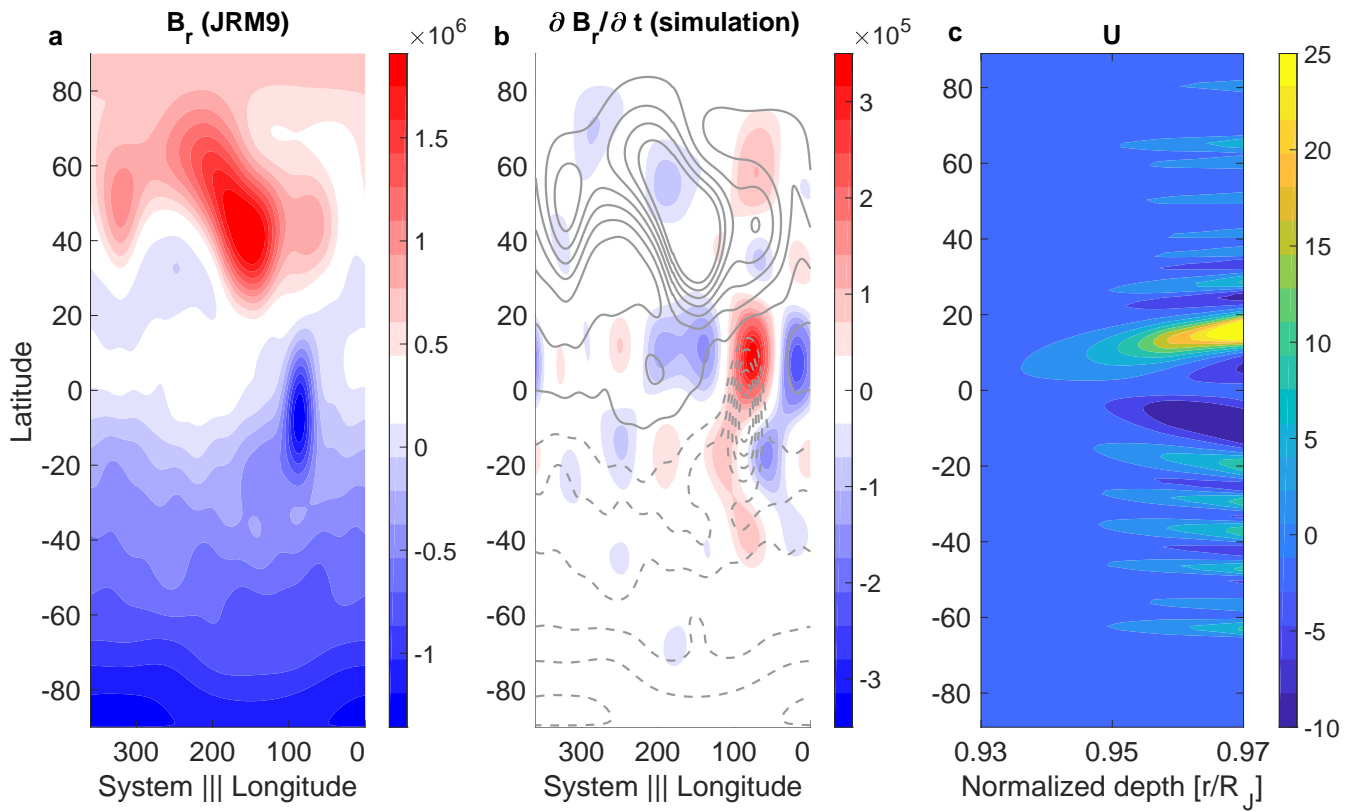


Figure 2: (a) The magnetic field [nT] measured from Juno’s first nine orbits (JRM9) at $\sim 0.972R_J$ (Connerney et al., 2018) (b) the changes in the magnetic field [$\text{nT} \cdot \text{yr}^{-1}$] caused by the simulated profile after 1 year at the same depth, with gray contours showing the measured magnetic field (JRM9) and (c) the simulated zonal flow as function of latitude and depth [ms^{-1}] at depths between $0.97R_J$ and $0.93R_J$. Both (a) and (b) are represented here with only 10 degrees and orders of the magnetic harmonic coefficients as in Connerney et al. (2018).

where neither model is sensitive (it is a non-conductive layer and the density anomalies are small), so this decay is not necessarily physically meaningful. For example, another more smoother solution can be constructed, that is optimized with less free parameters (Fig. 3a, light dashed red). This solution is more similar to the Kaspi et al. (2018) solution, but its ability to explain all the odd gravity harmonics is not as good as the best-fit solution (Fig. 3a, red). The four odd gravitational harmonics associated with this solution are: $J_3 = -1.71$, $J_5 = -6.83$, $J_7 = 9.86$ and $J_9 = -6.54$.

To make sure the combined best-fit solution fits also the MSV measurements, the magnetic field anomalies are recalculated from the new profile. The resulting magnetic field variation is almost identical to the variation from the MSV model solution alone. This confirms that the changes in the magnetic field are not sensitive to the flow structure above ~ 3000 km ($\cong 0.958R_J$). The gravity harmonics of the resulted decay profile are displayed in Table 1 (last column), the changes in the magnetic field are shown in Fig. 4b, and the gravity anomalies in Fig. 4c (blue). Fig. 4 also shows the simulated changes in the magnetic field (a) and the Juno measured gravity anomalies (c, red).

The method presented here provides a very good solution for the measurements created by the simulated profile, but should not be taken as a solution for Jupiter’s deep flows, since the magnetic field changes are based on our simulation and not the actual measurements. Once the magnetic measurements based on the following perijovs are available, the solution for the flow decay profile could be recalculated. Fitting these two independent measurements simultaneously will help to better constrain Jupiter’s deep flow structure.

4 Conclusions

So far, the Juno gravity measurements showed that cloud-level winds extend to a depth of about 3000 km (Kaspi et al., 2018). As the gravity field is mostly sensitive to density anomalies (and hence to flow strength) at depths of no more than a couple thousand kilometers, it is not possible to strongly constrain the strength of the flow below

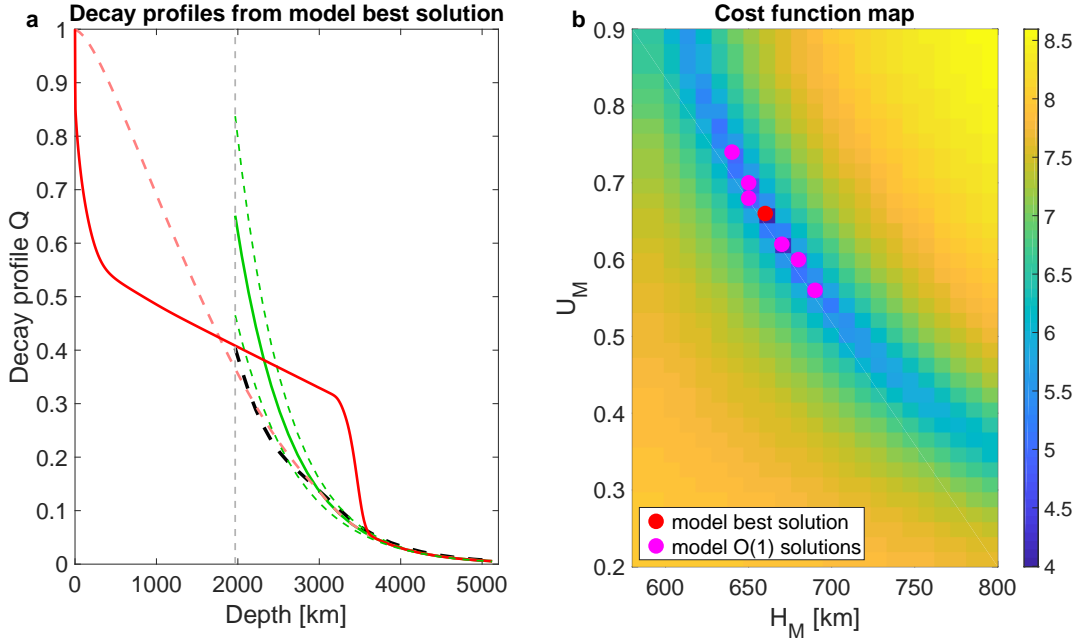


Figure 3: (a) The simulated decay profile (dashed black) together with the induction model solution for the lower region (green), its 3σ uncertainty (dashed green), the TW model solution for the upper region combining with the Induction solution below R_T (red) and an additional option for the combined solution (light dashed red); also shown is the induction model boundary at $0.972 R_J$ (dashed gray). Note that the induction model solution is very good below ~ 3000 km, in regions where the conductivity is high. (b) The cost function map for the induction model as function of the two optimized parameters: the exponential decay rate (H_M) and the flow strength at the induction model upper boundary relative to the surface flow (U_M). Also shown are the model best solution (red) and all solutions within $O(1)$ from it (pink).

that since the flow there is weak. Measurements of the time varying magnetic field of Jupiter might help to tackle this problem.

Here, we present a new combined method that uses two independent measurements from Juno to better resolve Jupiter’s internal flow structure. We use the thermal wind balance that relates the flow structure to the asymmetric gravity field, and the electromagnetic induction equation that explains changes in the measured magnetic field caused by the deep flow. Since the time varying magnetic field measurements are not available yet, we use the current gravity measurements and simulate changes in the magnetic field to find a decay profile that fits both. We find that the flow decay profile of Kaspi et al. (2018) is too strong at depths of more than ~ 3000 km and that further constraints must be added in order to fit both measured fields. We show that a decay profile that fits both the gravity measurements and the simulated magnetic measurements can be found through a joint optimization. Once the new magnetic measurements will be available we can reoptimize the solution to find a better flow structure.

We also find that J_3 is very sensitive to the deeper regions of the atmosphere while the MSV method limits the same region to low velocities, therefore posing upper and lower bounds for the flow velocity in the deep regions. The MSV method further constrains the deepest regions of the model such that strong flows cannot exist at all below ~ 4000 km, and nearly no flow (less than 1 ms^{-1}) can exist below ~ 5000 km. Finally, we find that the best solution is characterized with two rapid decays instead of one as in Kaspi et al. (2018), which could represent two distinct decay mechanisms for the flow, each at a different depth range.

Acknowledgments:

We thank H. Cao for providing the MSV code and for the very helpful discussions and suggestions. We also thank J.E.P. Connerney, J. Bloxham and R. Holme for very useful comments. This research has been supported by the Israeli Space Agency and the Helen Kimmel Center for Planetary Science at the Weizmann Institute of Science.

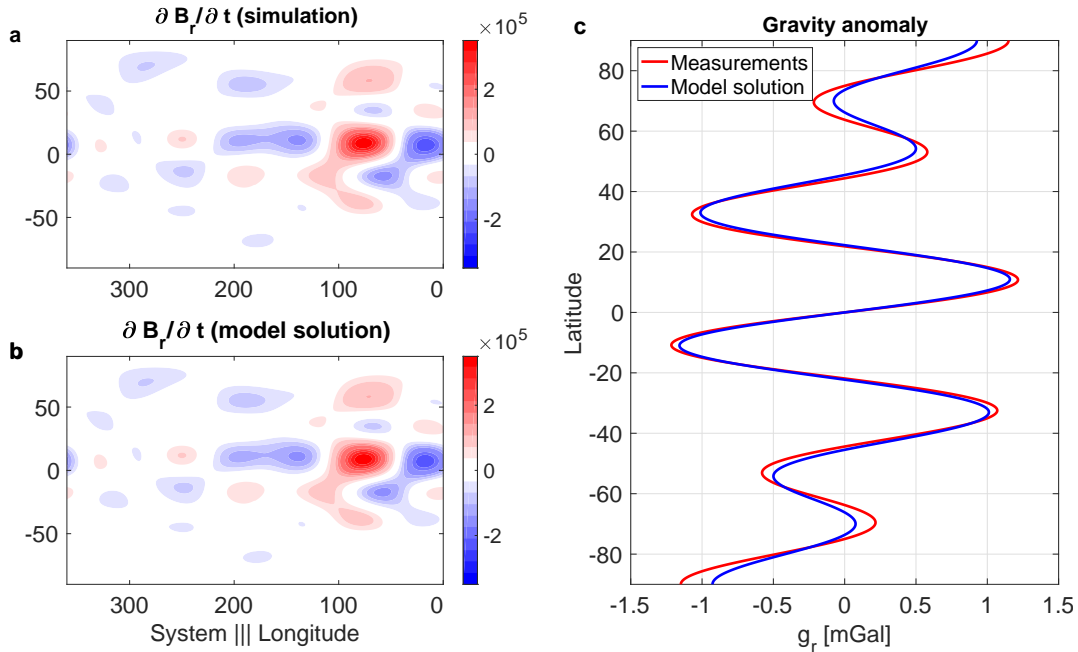


Figure 4: The combined gravity-magnetic solution. (a) The resulting time changes in B_r [$\text{nT} \cdot \text{yr}^{-1}$] from the simulation, (b) the model solution for the changes in B_r [$\text{nT} \cdot \text{yr}^{-1}$] after the same time span, and (c) the gravity anomalies as measured by Juno (red) and as calculated from the model best solution result (blue).

References

- Bloxham, J. (1992). The steady part of the secular variation of the Earth’s magnetic field. *Journal of Geophysical Research: Solid Earth*, 97(B13):19565–19579.
- Bloxham, J. and Gubbins, D. (1985). The secular variation of Earth’s magnetic field. *Nature*, 317:777–781.
- Cao, H. and Stevenson, D. J. (2017). Zonal flow magnetic field interaction in the semi-conducting region of giant planets. *Icarus*, 296:59–72.
- Connerney, J. E. P., Kotsiaros, S., Oliverson, R. J., Espley, J. R., Joergensen, J. L., Joergensen, P. S., Merayo, J. M. G., Hecceg, M., Bloxham, J., Moore, K. M., Bolton, S. J., and Levin, S. M. (2018). A new model of Jupiter’s magnetic field from Juno’s first nine orbits. *Geophys. Res. Lett.*, 45:2590–2596.
- Dietrich, W. and Jones, C. A. (2018). Anelastic spherical dynamos with radially variable electrical conductivity. *Icarus*, 305:15–32.
- French, M., Becker, A., Lorenzen, W., Nettelmann, N., Bethkenhagen, M., Wicht, J., and Redmer, R. (2012). Ab initio simulations for material properties along the Jupiter adiabat. *Astrophys. J. Sup.*, 202:5.
- Galanti, E., Cao, H., and Kaspi, Y. (2017). Constraining Jupiter’s internal flows using Juno magnetic and gravity measurements. *Geophys. Res. Lett.*, 44:8173–8181.
- Galanti, E., Durante, D., Finocchiaro, S., Iess, L., and Kaspi, Y. (2017). Estimating Jupiter’s gravity field using Juno measurements, trajectory estimation analysis, and a flow model optimization. *Astronom. J.*, 154(1):2.
- Galanti, E. and Kaspi, Y. (2016). An adjoint based method for the inversion of the Juno and Cassini gravity measurements into wind fields. *Astrophys. J.*, 820:91.
- Galanti, E. and Kaspi, Y. (2017). Deciphering Jupiter’s deep flow dynamics using the upcoming Juno gravity measurements and an adjoint based dynamical model. *Icarus*, 286:46–55.
- Galanti, E., Kaspi, Y., and Tziperman, E. (2017). A full, self-consistent, treatment of thermal wind balance on fluid planets. *J. Comp. Phys.*, 810:175–195.

- Gastine, T. and Wicht, J. (2012). Effects of compressibility on driving zonal flow in gas giants. *Icarus*, 219:428–442.
- Gastine, T., Wicht, J., Duarte, L. D. V., Heimpel, M., and Becker, A. (2014). Explaining Jupiter’s magnetic field and equatorial jet dynamics. *Geophys. Res. Lett.*, 41:5410–5419.
- Holme, R. and Olson, P. (2007). Large-scale flow in the core. *Treatise on geophysics*, 8:107–130.
- Hubbard, W. B. (2012). High-precision Maclaurin-based models of rotating liquid planets. *Astrophys. J. Lett.*, 756:L15.
- Iess, L., Folkner, W. M., Durante, D., Parisi, M., Kaspi, Y., Galanti, E., Guillot, T., Hubbard, W. B., Stevenson, D. J., Anderson, J. D., Buccino, D. R., Casajus, L. G., Milani, A., Park, R., Racioppa, P., Serra, D., Tortora, P., Zannoni, M., Cao, H., Helled, R., Lunine, J. I., Miguel, Y., Militzer, B., Wahl, S., Connerney, J. E. P., Levin, S. M., and Bolton, S. J. (2018). Measurement of Jupiter’s asymmetric gravity field. *Nature*, 555(7695):220–222.
- Jones, C. A. (2014). A dynamo model of Jupiter’s magnetic field. *Icarus*, 241:148–159.
- Jones, C. A., Boronski, P., Brun, A. S., Glatzmaier, G. A., Gastine, T., Miesch, M. S. and Wicht, J. (2011). Anelastic convection-driven dynamo benchmarks. *Icarus*, 216:120–135.
- Kahle, A. B., Vestine, E. H., and Ball, R. H. (1967). Estimated surface motions of the Earth’s core. *J. Geophys. Res.*, 72(3):1095–1108.
- Kaspi, Y., Flierl, G. R. (2007). Formation of jets by baroclinic instability on gas planet atmospheres. *J. Atmos. Sci.*, 64:3177–3194.
- Kaspi, Y. (2013). Inferring the depth of the zonal jets on Jupiter and Saturn from odd gravity harmonics. *Geophys. Res. Lett.*, 40:676–680.
- Kaspi, Y., Flierl, G. R., and Showman, A. P. (2009). The deep wind structure of the giant planets: Results from an anelastic general circulation model. *Icarus*, 202:525–542.
- Kaspi, Y., Galanti, E., Helled, R., Miguel, Y., Hubbard, W. B., Militzer, B., Wahl, S., Levin, S., Connerney, J., and Bolton, S. (2017). The effect of differential rotation on Jupiter’s low-degree even gravity moments. *Geophys. Res. Lett.*, 44:5960–5968.
- Kaspi, Y., Galanti, E., Hubbard, W. B., Stevenson, D. J., Bolton, S. J., Iess, L., Guillot, T., Bloxham, J., Connerney, J. E. P., Cao, H., Durante, D., Folkner, W. M., Helled, R., Ingersoll, A. P., Levin, S. M., Lunine, J. I., Miguel, Y., Militzer, B., Parisi, M., and Wahl, S. M. (2018). Jupiter’s atmospheric jet-streams extend thousands of kilometers deep. *Nature*, 555:223–226.
- Kaspi, Y., Hubbard, W. B., Showman, A. P., and Flierl, G. R. (2010). Gravitational signature of Jupiter’s internal dynamics. *Geophys. Res. Lett.*, 37:L01204.
- Kong, D., Zhang, K., Schubert, G., and Anderson, J. D. (2018). Origin of Jupiter’s cloud-level zonal winds remains a puzzle even after Juno. *Proc. Natl. Acad. Sci. U.S.A.*, 115(34):8499–8504.
- Liu, J., Goldreich, P. M., and Stevenson, D. J. (2008). Constraints on deep-seated zonal winds inside Jupiter and Saturn. *Icarus*, 196:653–664.
- Moore, K. M., Cao, H., Bloxham, J., Stevenson, D. J., Connerney, J. E., and Bolton, S. J. (2019). Time-variation of Jupiter’s internal magnetic field consistent with zonal wind advection. *Nature Astronomy*. In press.
- Moore, K. M., Yadav, R. K., Kulowski, L., Cao, H., Bloxham, J., Connerney, J. E., Kotsiaros, S., Jørgensen, J. L., Merayo, J. M., Stevenson, D. J., Bolton, S. J., and Levin, S. M. (2018). A complex dynamo inferred from the hemispheric dichotomy of Jupiter’s magnetic field. *Nature*, 561(7721):76–78.
- Nellis, W. J., Mitchell, A. C., McCandless, P. C., Erskine, D. J., and Weir, S. T. (1992). Electronic energy gap of molecular hydrogen from electrical conductivity measurements at high shock pressures. *Phys. Rev. Lett.*, 68(19):2937.
- Nellis, W. J., Ross, M., and Holmes, N. C. (1995). Temperature measurements of shock-compressed liquid hydrogen: implications for the interior of Jupiter. *Science*, 269(5228):1249–1252.

- Ridley, V. A. and Holme, R. (2016). Modeling the jovian magnetic field and its secular variation using all available magnetic field observations. *J. Geophys. Res. (Planets)*, 121(3):309–337.
- Tollefson, J., Wong, M. H., de Pater, I., Simon, A. A., Orton, G. S., Rogers, J. H., Atreya, S. K., C., R. G., Januszewski, W., Morales-Juberías, R., and S., M. P. (2017). Changes in Jupiter’s zonal wind profile preceding and during the Juno mission. *Icarus*, 296:163–178.
- Vallis, G. K. (2006). *Atmospheric and Oceanic Fluid Dynamics*. pp. 770. Cambridge University Press.
- Vestine, E. H. and Kahle, A. B. (1966). The small amplitude of magnetic secular change in the pacific area. *J. Geophys. Res.*, 71(2):527–530.
- Weir, S. T., Mitchell, A. C., and Nellis, W. J. (1996). Metallization of fluid molecular hydrogen at 140 GPa (1.4 mbar). *Phys. Rev. Let.*, 76:1860–1863.